Numerical investigation of air enclosed wave impacts in a depressurised tank

Z. H. Ma*, D. M. Causon, L. Qian, C. G. Mingham, P. Martínez Ferrer

Centre for Mathematical Modelling and Flow Analysis, School of Computing, Mathematics and Digital Technology, Manchester Metropolitan University, Manchester M1 5GD, United Kingdom

Abstract

This paper presents a numerical investigation of a plunging wave impact event in a low-filling depressurised sloshing tank using a compressible multiphase flow model implemented in open-source CFD software. The main focus of this study is on the hydrodynamic loadings that impinge on the vertical wall of the tank. The detailed numerical solutions compare well with experimental results and confirm that an air trapped plunging wave impact causes the vertical wall to experience pulsating pressure loadings in which alternate positive and negative gauge pressures occur in sequence following the first applied pressure peak. The strongest pulsations of the pressure are found to be near the air pocket trapped by the water mass. The instantaneous pressure distribution along the vertical wall is nearly uniform in the area contained by the air pocket. The phases of pulsating pressures on the wall are in synchronisation with the expansion and contraction of the trapped air pocket. The pocket undergoes changes in shape, moves upwards with the water mass and eventually breaks up into small parts. A careful integration of the wall pressure reveals that the vertical structure as a whole experiences pulsating horizontal impact forces. It is found that the average period of pulsation cycles predicted in the present study is around 5 ~ 6 ms, and the loading pulsations are quickly damped out in 0.1 ~ 0.2 s. Further exploratory investigation of the fluid thermodynamics reveals that the temperature inside the trapped air pocket rises quickly for about 2 ms synchronised with the pocket's first contraction, then the generated heat is rapidly transferred away in around 3 ms.

Keywords: naval engineering, computational fluid dynamics, breakwater

1. Introduction

Water waves impacting on fixed and floating structures are a major concern in coastal and ocean engineering. Violent wave induced impulsive loadings may damage coastal defence walls, break up oil platforms and dismantle large ships. In oceans, large waves under harsh weather conditions may impinge at the bow of a liquefied natural

*Corresponding author. Tel: +44 (0)161-247-1574
Email address: z.ma@mmu.ac.uk (Z. H. Ma)

gas carrier or other marine vessels and cause large forces and high frequency vibration. Green water slamming onto the deck may also cause severe damage. Meanwhile the liquid stored in a tank carried as cargo may undergo correspondingly violent motion resulting in strong wave impacts on the internal structure. The induced forces and moments may in turn cause significant changes in ship motions. These harsh hydrodynamic loadings represent a threat to the safety and stability of the vessel [1, 2].

With the fast development of computer technology and numerical analysis, computational fluid dynamics (CFD) has been more frequently used in coastal and ocean engineering to predict wave loadings on structures. Traditionally, potential flow theory is chosen to mathematically describe the dynamics of water waves assuming the flow to be irrotational [3]. However, the underlying assumption is not valid when the wave overturns, which introduces strong vorticity into the flow. Therefore new methods based on the one- or two-phase incompressible Navier-Stokes equations have been proposed to deal with viscosity, vorticity and air entrainment/entrapment for wave breaking problems [4, 5]. However fluid compressibility effects, which have a significant influence on the evolution of air trapping plunging waves observed in experiments [6–10], still cannot be properly handled by these incompressible models. This requires a more detailed compressible multiphase flow model that can include all necessary physics to provide an accurate solution [11].

Recently researchers have started to explore the importance of fluid compressibility in numerical simulations of wave impacts by using the volume of fluid (VOF) method to capture the free surface. Bredmose *et al.* [12, 13] proposed a weakly compressible flow model to compute wave impact events. A density-based numerical method employing an iterative Riemann solver was used to solve the conservative flow model. However benchmark tests of a one-dimensional shock wave passing through a water-air interface exhibited strong non-physical pressure oscillations at the material interface. Plumerault *et al.* [14] proposed a density-based compressible three-fluid model for describing aerated-water wave problems. Nevertheless it is noted that strong non-physical oscillations also arose at the material interface in their water-air shock tube results [14]. When this model was used to simulate a plunging wave impact problem, non-physical numerical oscillations occurred in the computation [15]. This caused the impact pressure to keep oscillating without decaying, which is contrary to the phenomenon observed in experiments that the impact loads were quickly damped out [8].

Bredmose *et al.* [12, 13] and Plumerault *et al.* [14, 15] did not clarify the underlying reason causing the non-physical numerical oscillations in their computations. However, Ma *et al.* [16] have pointed out that the non-physical oscillations are due to the use of fully-conservative flow models in their numerical calculations of multiphase flows. Instead of using a fully-conservative flow model, they proposed a quasi-conservative compressible two-phase flow model building on the conservation laws and a non-conservative advection equation for the volume fraction [16]. A

density-based method adopting a HLLC-type approximate Riemann solver was applied to solve the multiphase flow model. The method exhibited good numerical conservation behaviour and the non-physical pressure oscillations were effectively removed in water-air shock tube tests. The method has also been successfully extended to solve incipient cavitations and underwater explosions [17] as well as violent water entry of rigid flat plates under various aeration conditions [18]. However, difficulties still arose in computing plunging wave impact problems as the pressure did not decay but kept ringing with a relatively large amplitude.

Although an initial study of the reported works of Bredmose *et al.* [12, 13], Plumerault *et al.* [14, 15] and Ma *et al.* [16] gives an impression that these flow models were properly constructed and suitable for wave impact problems, the implausible results for either the water-air shock tubes or plunging wave impact problems implies that some very important aspects of the numerical algorithms remain unresolved in these works. It is noted that standard density-based methods were adopted by all of them to solve wave impact problems no matter what kind of multiphase flow models (fully-conservative or quasi-conservative) were used. Apparently these authors ignored the fact that density-based methods are not suitable to solve nearly incompressible low-speed (low-Mach) flows without applying special treatments to overcome the system stiffness problem.

It is well-known that density-based methods were originally designed for high-speed compressible flows. In this context, the continuity equation is used to obtain the density field while the pressure field is determined from the equation of state. However for low-speed flows, pressure is weakly coupled or even decoupled from density. This causes convergence difficulties for density-based methods. With a non-convergent solution to steady flows, the variation of pressure between successive time steps may well exceed the whole range of the real physical pressures [19]. It will become even worse for unsteady low-speed flows, which require an accurate computation of the pressure field at every real time step.

As a matter of fact, the impact of a plunging wave with enclosed air pocket is rather complicated. The flow consists of a small but remarkable compressible region (the air pocket) and a much larger low-speed (low-Mach) incompressible area (the water and air outside the enclosed air pocket) as shown in figure 1. To properly handle this kind of problem, numerical methods must closely follow the physics by taking the following important factors into account:

- The flow is not single-phase but multi-phase.
- The flow includes incompressible and compressible regions.
- The enclosed air pocket repeatedly contracts and expands.
- Standard density-based methods are not suitable for low speed flows.

To solve low-speed flows with density-based methods, preconditioning of the governing equations by pre-multiplying

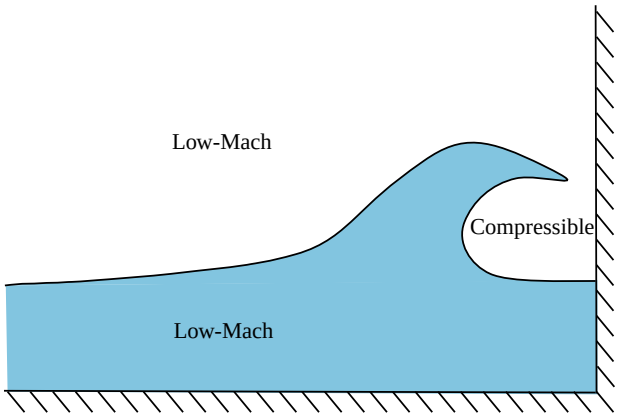

Figure 1: A sketch of an air-enclosed plunging wave impact at a vertical wall. The flow domain consist of compressible and low-speed (nearly) incompressible regions.

time derivatives with a suitable matrix is a popular option to address the system stiffness problem. Unfortunately the resultant accuracy and convergence rate depend upon the choice of artificial parameters. Moreover this becomes extremely complicated especially when multiphase flows are considered [19, 20]. To the knowledge of the authors, a density-based conservative method suitable to solve air enclosed wave impacts with proper modifications to improve the low-speed region computation is not available yet. On the other hand, pressure-based methods, which sequentially solve the momentum equations and the pressure correction equation in an iterative process, can properly deal with low-speed incompressible flows. These methods have been successfully extended to incorporate compressibility for single-phase aerodynamic flows [21–23] and multi-phase cavitating flows [24].

The objective of the present work is to investigate air-enclosed plunging wave impact loads on structures with an appropriate numerical method. This includes the following important aspects:

- the evolution of the free surface and enclosed air pocket,
- air cushion effects on the spatial distribution of pressure loadings,
- the repeated contraction and expansion of the air pocket,
- the alternation of super- and sub-atmospheric local pressures,
- the overall force/momentum on the structure.

As is emphasised, a suitable numerical method needs to be capable of dealing with both compressible and incompressible regions for plunging wave impact problems. Apparently density-based numerical models proposed by Bredmose *et al.* [12, 13], Plumerault *et al.* [14] and Ma *et al.* [16] are not ready yet as these codes have not implemented the necessary low-speed treatments. Besides these VOF based methods, researchers have also devoted efforts to develop particle based Lagrangian methods e.g. smooth particle hydrodynamics (SPH) to deal with free surface problems. Im-

portant contributions to the development of compressible multiphase SPH methods include the works of Colagrossi and Landrini [25], Colagrossi *et al.* [26], Guilcher *et al.* [27, 28], and Rafiee *et al.* [29] and references therein. While these studies did not give a discussion of the issues raised by the authors i.e. the multi-speed problem regarding incompressible and compressible regions as well as the alternate contraction and expansion (not solely compression) of the enclosed air pocket. Hence it is uncertain whether the concerns raised in the present work could be fully addressed by these particle methods. Therefore here we seek an alternative approach to solve the plunging wave impact problems by using pressure-based numerical methods which have been appropriately extended to the compressible regime.

In order to focus our attention on analysing the underlying physics of air-enclosed plunging wave impacts we do not intend to develop a computer model from scratch but to use and modify as appropriate the open-source code OpenFOAM, which provides multiple choices including single- and multi-phase incompressible and compressible flow solvers. We choose the component package *compressibleInterFoam* to deal with compressible air and water free surface flows. To the knowledge of the authors, this solver has not been rigorously validated for hydrodynamic wave impact problems regarding its efficacy and conservation properties. Therefore, our first task in the present work is to evaluate the efficacy and conservation properties of this solver by using a benchmark test case of a half-filled smooth sloshing tank without impact. Then, the solver is extended to calculate much more complicated air enclosed plunging wave impact problems in a low-filling depressurised tank.

The remainder of the paper is organised as follows. The mathematical model and numerical solution scheme are presented in Section 2. A verification of the capability of the solver *compressibleInterFoam* to deal with a smooth sloshing tank case without impact is carried out in Section 3. In Section 4 the code is utilised to solve air enclosed wave impacts in a depressurised tank. The obtained solution is compared to experiments as well as incompressible computations. Final conclusions are drawn in Section 5.

2. Numerical model

The fundamental mathematical equations of the two-phase flow model *compressibleInterFoam* consist of the conservation laws of mass, momentum and energy as well as a transport equation for the water volume fraction. The fluid flow mixture of water and air is assumed to be homogeneous and the two components are assumed to be in mechanical equilibrium with identical velocity and pressure. The volume fraction for the water component is given by

$$\alpha = \frac{\Omega_{\text{water}}}{\Omega_{\text{water}} + \Omega_{\text{air}}} \tag{1}$$

The mixture density is then given by

$$\rho = \alpha\rho_{\text{water}} + (1-\alpha)\rho_{\text{air}}, \tag{2}$$

and the viscosity is given by

$$\mu = \alpha\mu_{\text{water}} + (1-\alpha)\mu_{\text{air}} \tag{3}$$

2.1. Governing equations

The mass conservation equation is given by

$$\frac{\partial\rho}{\partial t} + \nabla\cdot(\rho\mathbf{U}) = 0, \tag{4}$$

in which $\mathbf{U}$ represents the velocity vector. The momentum equation is given by

$$\frac{\partial\rho\mathbf{U}}{\partial t} + \nabla\cdot(\rho\mathbf{U}\mathbf{U}) - \nabla\cdot(\mu\nabla\mathbf{U}) = \sigma\kappa\nabla\alpha - \mathbf{g}\cdot\mathbf{x}\nabla\rho - \nabla p_{\text{d}}, \tag{5}$$

where σ is the surface tension coefficient; the curvature of the interface is calculated as $\kappa = \nabla\cdot(\nabla\alpha/|\nabla\alpha|)$; $p_{\text{d}} = p - \rho\mathbf{g}\cdot\mathbf{x}$ is the dynamic pressure; $\mathbf{g}$ is the gravitational acceleration and $\mathbf{x}$ is the position vector. An energy equation expressed in terms of temperature T is given by

$$\frac{\partial\rho T}{\partial t} + \nabla\cdot(\rho\mathbf{U}T) - \nabla\cdot(\mu\nabla T) = -\left(\frac{\alpha}{c_{\text{v,water}}} + \frac{1-\alpha}{c_{\text{v,air}}}\right)\left(\frac{\partial\rho k}{\partial t} + \nabla\cdot(\rho\mathbf{U}k) + \nabla\cdot(\mathbf{U}p)\right), \tag{6}$$

in which $k = |\mathbf{U}|^2/2$ is the specific kinetic energy; $c_{\text{v,water}}$ and $c_{\text{v,air}}$ are the specific heat capacities at constant volume for the water and air phases, respectively. A transport equation for the water volume fraction used to capture the free surface is given by

$$\frac{\partial\alpha}{\partial t} + \mathbf{U}\cdot\nabla\alpha + \nabla\cdot\mathbf{U}_c\alpha(1-\alpha) = 0, \tag{7}$$

where $\nabla\cdot\mathbf{U}_c\alpha(1-\alpha)$ is an anti-diffusion term utilised to sharpen the interface.

The density of air is correlated with the pressure p and the temperature T by the following perfect gas equation of state

$$p = \rho_{\text{air}}R_{\text{air}}T, \tag{8}$$

in which $R_{\text{air}} = 287$ J/(kg·K) is the specific gas constant. The water is treated as a barotropic fluid with the following equation of state

$$\rho_{\text{water}} = \rho_{0,\text{water}} + \psi(p - p_0), \tag{9}$$

in which $\rho_{0,\text{water}}$ is the initial density of water corresponding to the initial pressure p_0, $\psi = 1/(R_{\text{water}}T)$ is a compressibility coefficient, and $R_{\text{water}} = 3000$ J/(kg·K) is used in the present work.

2.2. *Solution algorithm*

The complete two-phase flow model includes the conservation laws represented by equations (4), (5) and (6) as well as the water volume fraction transport equation (7). All these equations are discretised by a finite volume method on collocated grids and the transient flow problem is solved by the PISO method [30]. The fundamental procedure to solve the compressible two-phase flow model with PISO method is listed in Algorithm 1.

Algorithm 1: *compressibleInterFoam* solution procedure

begin Time advancement
- **begin** PISO loop
  - Solve transport equation (7) for water volume fraction α;
  - Solve mass continuity equation (4);
  - Solve momentum equation (5);
  - Solve energy equation (6);
  - Fixing the pressure, update ρ_{air} and ρ_{water} through EOS (8) and (9), respectively;
  - **begin** Pressure correction loop
    - Correct the pressure;
    - Fixing the temperature, update ρ_{air} and ρ_{water} through EOS (8) and (9), respectively;
    - Update the mixture density ρ through equation (2) ;
  - **end**
- **end**

end

3. Validation

A test case of a smooth sloshing tank without impact is firstly chosen to validate the open-source code *compressibleInterFoam*. Figure 2 shows the setup for this problem, in which a half-filled square tank of 0.6 m wide oscillates horizontally with a sinusoidal law, $x = A(1 - \cos\omega_0 t)$. The experiment was carried out by Koh *et al.* [31] with an excitation amplitude $A = 5$ mm and the fundamental (natural) frequency of the sloshing wave $\omega_0 = 6.85$ rad/s. The ullage pressure in the tank is set to be 1 bar. A pressure transducer P_1 is installed on the left side wall above the tank bottom at a distance of 20 mm. A free surface gauge H_1 is located in the middle between the ceiling and floor at a distance of 20 mm to the right side wall.

A numerical convergence study is carried out on three successively refined uniform meshes with 50×50, 100×100 and 200×200 cells. The time step is fixed to be $\Delta t = 1$ ms on all the meshes for comparison purposes. The total physical time for the numerical simulation is 9 s. All the boundaries are treated by an adiabatic no-slip solid wall condition. Figure 3 gives several snapshots of the free surface at times t =3.45, 3.9, 7.65 and 8.6 s. The wave runs up and down along the vertical wall without breaking throughout the whole process. Figure 4 shows the corresponding instantaneous pressure contours in the sloshing tank. It may be observed that the distribution of computed pressure is smooth, which is superior to some particle methods like MPS [31].

Figure 5 and 6 illustrate the free surface displacements at H_1 and ullage pressure series at P_1, respectively. The red, purple and black lines are the present numerical results obtained on the three successively refined meshes. The green dashed lines represent the independent calculations of Bai *et al.* [1] using a level-set based incompressible two-phase flow model. The empty bullets are the experimental measurements of Koh *et al.* [31]. Discrepancies between the results of Bai *et al.* [1] and the experiment [31] can be noted after $t = 6.5$ s in the peak/trough values of the free surface displacement and gauge pressure as well as the associated phases. One possible reason for these discrepancies might be due to the non-conservative property of the level set method adopted by Bai *et al.* [1], which was not clarified by these authors. Looking at the present computation, good convergence is established on the fine mesh with 100×100 cells. It is also clearly shown that the present converged solutions agree well with the experiment results of Koh *et al.* [31].

Additionally, the mass conservation property of the code *compressibleInterFoam* is also investigated in the present work. We calculate the ratio of mass error as $M_{\text{error}} = (M_t - M_0)/M_0 \times 100\%$, in which M_0 is the intial total mass in the tank and M_t is the mass at time t. The computed mass errors on the three successively refined meshes are shown in figure 7. On all the meshes, the mass error are zero throughout the whole simulation.

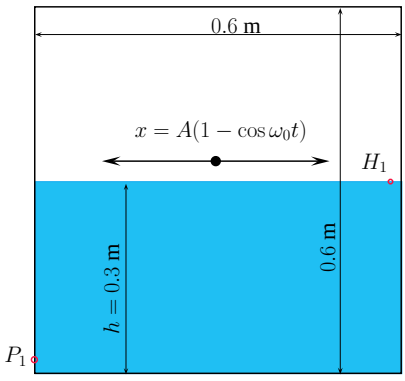

Figure 2: Setup of the sloshing tank. The length of the square tank is 0.6 m and it is partially filled with water of depth 0.3 m. The tank has a pure horizontal motion (sway) with a sinusoidal law, $A(1 - \cos\omega_0 t)$. A=5 mm, ω_0=6.85.

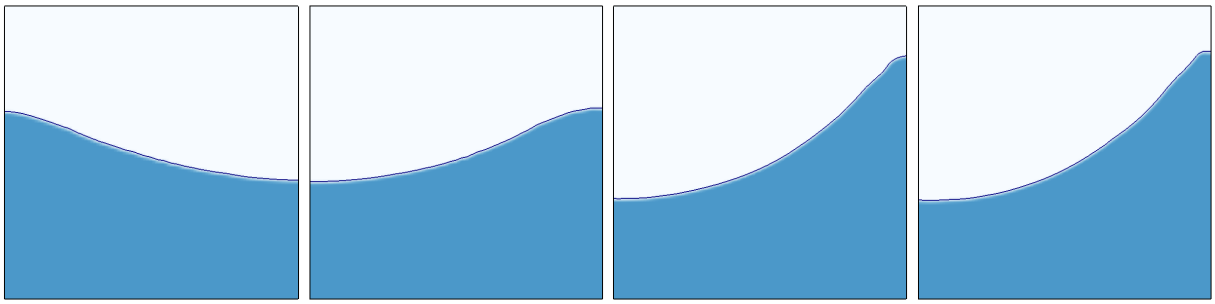

(a) t=3.45 s (b) t=3.9 s (c) t=7.65 s (d) t=8.6 s

Figure 3: Snapshots of the free surface profile in the square sloshing tank.

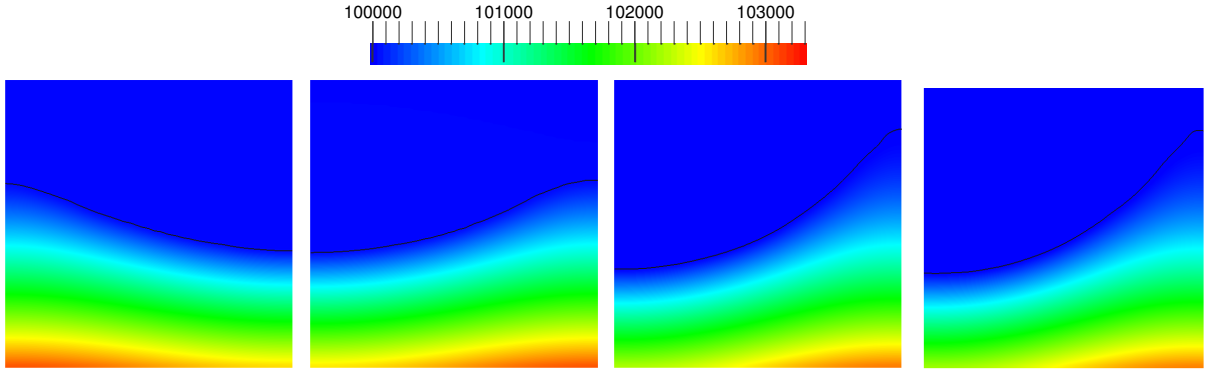

(a) t=3.45 s (b) t=3.9 s (c) t=7.65 s (d) t=8.6 s

Figure 4: Snapshots of the total pressure distribution in the square sloshing tank (Units in Pa).

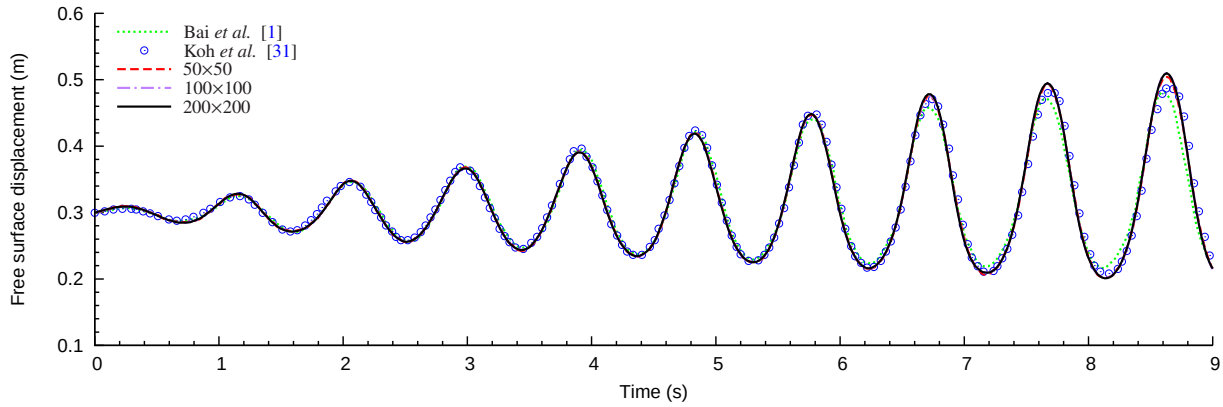

Figure 5: Time history of the free surface displacement at point H_1. The dashed green line represents the numerical solution of Bai *et al.* [1]. The circles indicate the experimental measurements of Koh *et al.* [31]. The red, purple and black lines are the present numerical results obtained with *compressibleInterFoam* on the three successively refined meshes.

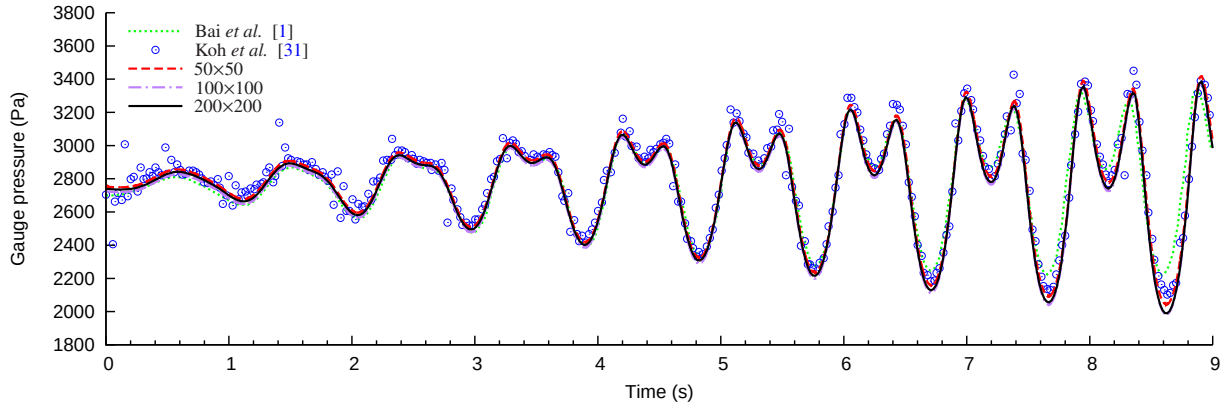

Figure 6: Time history of the gauge pressure at point P_1. The dashed green line represents the numerical solution of Bai *et al.* [1]. The circles indicate the experimental measurements of Koh *et al.* [31]. The red, purple and black lines are the present numerical results obtained with *compressibleInterFoam* on the three successively refined meshes.

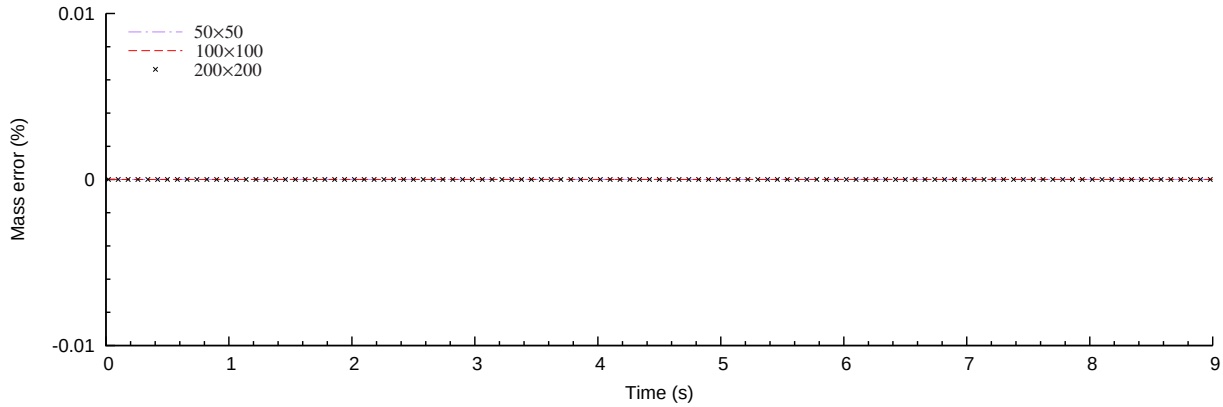

Figure 7: Mass conservation on the three successively refined meshes. The ratio of mass error is calculated by $M_{\text{error}} = (M_t - M_0)/M_0 \times 100\%$, in which M_0 is the initial total mass in the sloshing tank and M_t is the mass at time t. The red dashed line is on top of the purple dash-dot line.

4. Air-enclosed plunging wave impact

Here we focus on the simulation of an air-enclosed plunging breaker impact in a depressurised tank. Figure 8 shows the setup of this problem, in which the length of the square tank is 1 m, the filling depth is 0.125 m. The tank oscillates in the horizontal direction with a sinusoidal law, $x = A\sin(2\pi t/T)$. The excitation amplitude is $A = 3$ cm and the period of sway motion is $T = 1.6$ s. The ullage pressure in the tank is set to $p_0 = 0.75$ bar. Several pressure transducers are installed on the left side wall of the tank located at $y = 5$, 25, 45, 65 and 85 mm (from the free surface). The experimental study was carried out by Lugni *et al.* to analyse the kinematics [9] and dynamics [8] of wave impact.

To precisely capture the important flow features especially the air pocket trapped in the water mass we use a non-uniform fine mesh to discretise the domain. The horizontal direction of the tank is uniformly divided with 500 mesh cells. In the vertical direction, the lower part (40%) and upper part (60%) of the tank are regularly discretised by 200 cells and 60 cells, respectively. The time step is fixed to be $\Delta t = 10\ \mu$s throughout the numerical simulation in order accurately to resolve the transient phenomenon of wave impact. All the boundaries are treated with an adiabatic no-slip solid wall condition. Lugni *et al.* [8] did not clarify the environmental temperature for their experiments, while it is initially set to be 15°C everywhere in the present work. In addition to the compressible two-phase code *compressibleInterFoam*, an incompressible two-phase code *interFoam* included in the OpenFOAM library is also used to calculate the flows with the same mesh and boundary conditions.

4.1. Propagation of the free surface

As is known, when the crest velocity is larger than the phase speed, the wave cannot sustain its stable profile any longer. The crest will try to catch up with the trough in front of it with an acceleration. If the acceleration is large enough, the crest will curl over and drop onto the trough of the wave thus forming a plunging breaker. This kind of breaking wave can enclose air pockets in the water mass. A detailed description of the kinematics including the free surface evolution associated with the plunging breaker impacting on a vertical wall of the sloshing tank can be found in the work of Lugni *et al.* [8]. For completeness, the propagation of the free surface is briefly described here too. Figure 9 presents several snapshots of the plunging wave profile near the moment of impact with the vertical wall. When the wave crest overturns and approaches the wall, the trough also quickly moves upward with a large acceleration. The wave creates a fast spray from the crest and breaks up violently on the wall. The trapped air pocket is compressed by the water mass and moves upward along the wall. The shape of the air pocket undergoes a change from half-cylinder to half-ellipse and the pocket volume decreases (contraction) and increases (expansion) with time.

The computed free surface profiles are similar to the experimental results of Lugni *et al.* [8] while we also notice there are some differences between them. The break up spray released from the wave crest could not be appropriately

reproduced by the numerical code from $t = t_0 - 6$ ms to $t = t_0 + 1.5$ ms, in which t_0 represents the time at which the impact pressure reaches its first and highest peak value. Thus the trapped air cavity is closed earlier with a larger volume in the experiments than in the simulations. This may be due to a possible tiny under- or over-shoot of the tank excitation amplitude in the experiments or due to the non-smooth acceleration of the tank. The differences in the kinematics may accumulate with time causing the aforementioned discrepancies for this highly non-linear hydrodynamic problem. As a matter of fact, Lugni *et al.* pointed out that the repeatability of the kinematics and dynamics is relatively low for this case [8, 9].

4.2. Local pressures and overall force

Figure 10 gives an overview of the computed gauge pressure at P_3 and the ratio of mass error obtained by *compressibleInterFoam* and *interFoam*. Both the incompressible and compressible solvers obey the mass conservation law quite well. A first glance would also suggest that *interFoam* and *compressibleInterFoam* produce similar results in respect of the pressure loadings. However, a discrepancy between the two solvers may be observed at a time around $t = t_0$ when a plunging wave impact event occurs.

A detailed comparison of the impact (gauge) pressure loadings on the vertical wall obtained by the numerical simulations and experiments is presented in figure 11. The dashed lines represent the solution of *interFoam*, the red lines are the results of *compressibleInterFoam* and the black lines are the experimental measurements of Lugni *et al.* [8]. Please note that the phases of all results have been shifted to correlate the first peak to time zero. We would also like to point out that the numerical pressure sensor P_5 is placed at the spray root $y = 65$ mm; the other numerical sensors are placed below it with a successive decrease of 20 mm. In the experiments [8], the transducer P_5 was located at the spray root $y = 85$ mm.

At P_4, the amplitude of the first pressure peak computed by *compressibleInterFoam* is 16.6 kPa, which is close to the measurement of 17.7 kPa, while *interFoam* provides a relatively small value of 13.2 kPa. Considering the rise time of this peak, there is a difference of about 2 ms between the experiment and numerical computations. At all the other gauge locations, the measured rise time of the pressure peaks is always larger than the computed ones, while the difference seems to shrink with depth; the pressure peaks predicted by *compressibleInterFoam* are close to the measurements, *interFoam* gives a lower prediction of pressures at all locations. After the first peak, both the experiment and *compressibleInterFoam* show a continuous decline of the pressure towards negative values, which is synchronous with the expansion of the trapped air pocket. However, the repeated physical expansion and contraction of the air pocket could not be handled by *interFoam* since it treats the air as an incompressible fluid with a constant density. In consequence, the pressures calculated by *interFoam* remain positive throughout the simulation. As a matter of fact, the trapped air pocket undergoes expansion and contraction alternately leading to the pulsating pressure

loadings on the vertical wall, which is clearly illustrated by the experimental measurements and the compressible numerical results. It is also clearly shown in the figure that the pulsations of pressure at different locations are almost synchronous for the experimental measurements. Besides, the pressures computed by *compressibleInterFoam* at all gauge points also go up and down synchronously. However, the incompressible two-phase code failed substantially to resolve this complex physical phenomenon. This indicates that the fluid compressibility plays a crucial role in this kind of impact problem.

We also notice that after the second period of pressure pulsation ($t = 0.01$ s), *compressibleInterFoam* starts to show a difference in phase with the experiment. The pressures seem to be damped more quickly and effectively in the experiments compared to the compressible computations. From time zero to $t = 0.05$ s, the averages of pressure pulsation periods for the measured data and the compressible computation are 5 ms and 6 ms, respectively. There are several possible reasons for this difference. One is the potential side wall effect in the experiments; the two side walls enclosing the tank in the third (z) direction with a distance of 10 cm produce friction/turbulence that may dampen the fluid flow energy [32]. Another reason might be due to the 3D effects in the experiment, a part of the air is leaked from the trapped pocket in experiment since the pocket cannot be perfectly wrapped by the vertical wall and highly irregular free surface during this strong hydrodynamic impact. This leads to the loss of energy and air mass in the pocket [8, 32]. The current computations are purely 2D, therefore side wall effects and any free surface 3D irregularity are not included. Of course, the different initial trapped volumes of the air pockets could also cause the phase shift between the computed and measured pressures.

A frame-by-frame analysis of the computed pressure distribution in the flow field at a peak or trough for the first six pulsation cycles is presented in figure 12. It is interesting to note that the distribution of pressure along the vertical wall has the shape of a pointed hand gun at $t = 0$. The highest pressure occurs at the impact point of the wave "tongue" (spray root). Below this "tongue" in the air pocket, the pressure has a plateau indicating a uniform loading distribution along the wall. This also implies that the air pocket undergoes isotropic contraction at this stage. Below the air pocket, the pressure decreases from 16.6 kPa to 8.7 kPa with depth in a parabolic relationship. All the pressures gauged in water are positive. The pressure distribution along the wall changes abruptly with the expansion of the air pocket. At the first pressure trough, the pressures in the air pocket are negative and nearly uniform along the wall. The negative pressures are not limited to the air pocket only but have a broader influence area including the upside spray root and the downside wall. The pressure at the spray root is greatly reduced by the influence of the pocket. Below the air pocket, the pressure gradually increases with water depth. At this moment, the integral of gauge pressure along the wall is negative. This implies that the wall as a whole may experience a rightward (pull) force if all the other force contributions from the external atmosphere and neighbouring attached walls remain constant. In

the following ten frames, it is easy to note that the pressure in the air pocket becomes positive and negative alternately and this influences a large area in the tank with synchronised pressure pulsation. During the upward movement, the air pocket breaks up into two parts. It is also interesting to note that small peaks are superimposed over the air pocket pressure at either end of the pressure plateaus for t =0, 3 ms, 6 ms and 9.75 ms in the figure. These are related to the hydrodynamic pressures at the root of the water sprays from the wave crest or trough.

Figure 13 provides a time-continuous view of the computed gauge pressures on the wall for $t = -0.02$ s to 0.1 s (the upper graph). As is shown in the figure, the maximum impact pressure illustrated by the red area is local in both space and time. The minimum pressure occurs after the first peak and influences a much broader area in addition to the small air pocket. The dark blue areas represent negative pressure loadings in coincidence with the expansion of the trapped air pocket. The peak and trough values of pressure spread upwards along the wall and decay quickly with time in only about 0.1 s. For comparison purposes, the experimental results of Lugni *et al.* [8] for gauge pressures on the wall are also included in the figure (the lower graph). The (dark) grey areas represent measured positive pressures, while the white parts indicate negative pressures. It is clearly shown that positive and negative gauge pressures occur alternatively and the negative pressures have a broader influence area than the small air pocket. The pressure pulsations were damped out quickly when spreading upwards along the wall. The whole trend of the computed solution is quite similar to the experimental measurement.

As mentioned before, the integral of the gauge pressure on the wall at a trough time frame may be negative, and becomes positive at a peak time. This implies that the overall horizontal force on the vertical wall induced by the plunging wave impact may pulsate in synchronisation with the contraction and expansion of the trapped air pocket. Unfortunately this was not clarified or even investigated in the experimental study of Lugni *et al.* [8]. One reasonable explanation may be that it was impossible to install a load cell or adequate pressure transducers on the vertical tank wall properly to measure the fluid impact force. In order to verify our speculation regarding the force, we assume the vertical wall of the 2D sloshing tank has a width of 1 m in z-direction and then integrate the absolute pressure on this wall. The calculated horizontal wave impact forces are depicted in figure 14, in which the red lines present the results of *compressibleInterFoam* and the dashed blue lines are the results of *interFoam*. The left part of this figure gives an overview of the wave impact forces for $t = -0.5$ s to 1 s. A simple sketch of all the horizontal forces acting on the wall is also provided, in which F_{i} is the wave impact force; F_{a} is the external atmospheric force acting on the wall; F_{t} and F_{b} are the friction provided by the ceiling and floor of the tank. During the sloshing process, none of these force contributions remains constant as a matter of fact. It is clearly shown in this figure that the wave impact force has a strong pulsation from $t = 0$ to 0.05 s. The pulsation is then quickly damped out and the impact force converges to the hydrostatic value. It is interesting to note that the peak force calculated by *interFoam* is

lower than *compressibleInterFoam*. The incompressible code completely fails to capture the important force pulsation after the first peak. Nevertheless, the force predicted by *interFoam* seems to give a reasonable representation of the neutral/averaged value of these pulsations.

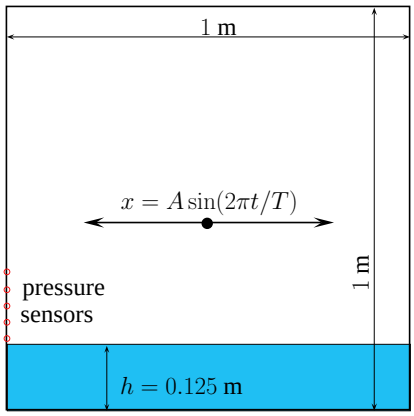

Figure 8: Setup of the depressurised sloshing tank. The length of the square tank is 1 m and it is partially filled with water of depth 0.125 m. The tank has a pure horizontal motion (sway) with a sinusoidal law, $A\sin(2\pi t/T)$. A=3 cm, T=1.6 s. The ullage pressure in the tank is p_0=0.75 bar.

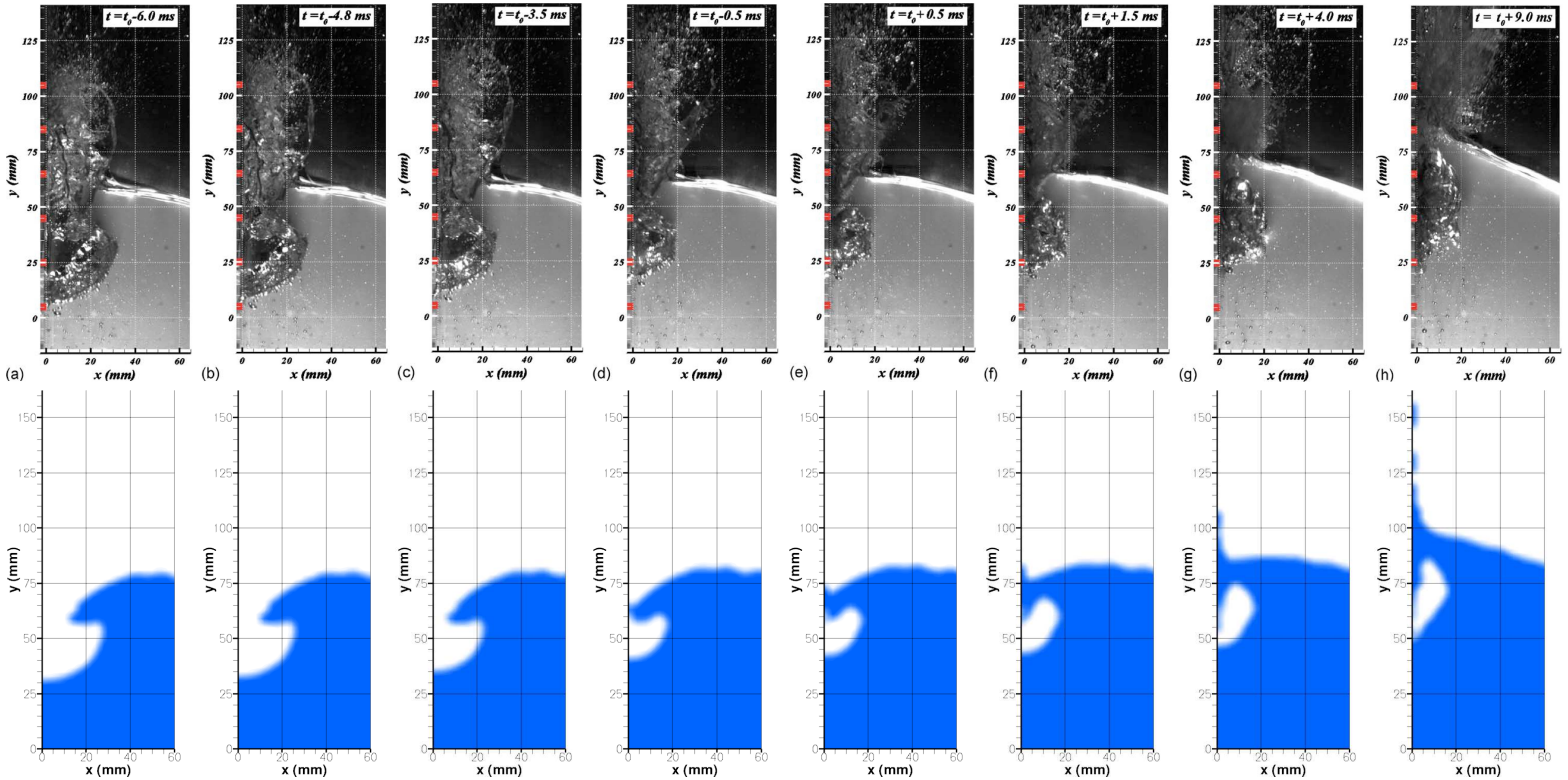

Figure 9: Evolution of the plunging breaker near the moment of impact. Upper: the experimental results of Lugni *et al.* [8]; lower: the present computed solution of *compressibleInterFoam*.

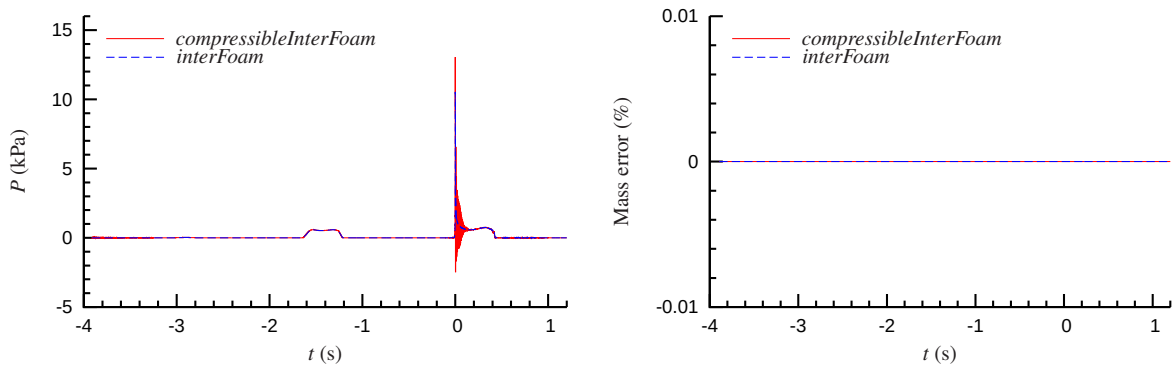

Figure 10: Comparison of the computed results of *compressibleInterFoam* and *interFoam* for $t = 0 \sim 5$ s. Left: gauge pressure at P_3; right: mass conservation error. The solid line represents the solution of *compressibleInterFoam* and the dashed line is the calculation of *interFoam* .

4.3. Thermodynamic characteristics

In the past, there is hardly any evidence in the literature showing that structures subject to air enclosed plunging waves were excessively heated during these violent impacts. In consequence, very limited attention was paid to the thermodynamic behaviour of the trapped air pocket and surrounding water. One underlying reason is due to the large heat capacity of water, which enables it to transfer heat rapidly and effectively. Thus a detailed or even explorative experimental measurement of temperature variations for plunging wave problems has not been reported in the literature so far. However, Abrahamsen and Faltinsen pointed out, based on their theoretical analysis, that heat exchange modifies the stiffness of the air pocket and dampens the pulsations, and they believe this factor is important for air pocket slamming events including an overturning wave trapping an air pocket at a vertical wall [32].

The compressible model utilised in the present work actually includes the energy equation, and this enables it to deal with the thermodynamics. During the numerical computations, we record the temperatures at the gauge points $P_1 \sim P_5$ in addition to the pressures. Figure 15 shows the temperature variations at these points. It is interesting to note that the temperature remains almost constant in most places; only the temperature in the air pocket undergoes significant change. At P_4, the computed temperature rises quickly by more than 16 degrees in the compression phase of the pocket, which lasts for about 2 ms. It then drops dramatically in the following expansion phase of the pocket by about 22 degrees. Finally, the temperature recovers to the environmental value without further pulsation.

Figure 16 provides a time-continuous view of the temperature variations on the vertical wall for $t = -0.01 \sim 0.04$ s. This again demonstrates the fast evolution of temperature in the trapped air pocket. Unlike the pressure having a much broader influence area and multiple pulsations, the temperature has a quite confined influence area with only one pulsation, which lasts for only about 5 ms. Obviously, the rapid transition of temperature is a big challenge to most of the temperature measurement devices available in laboratory experiments. In order to disclose the real

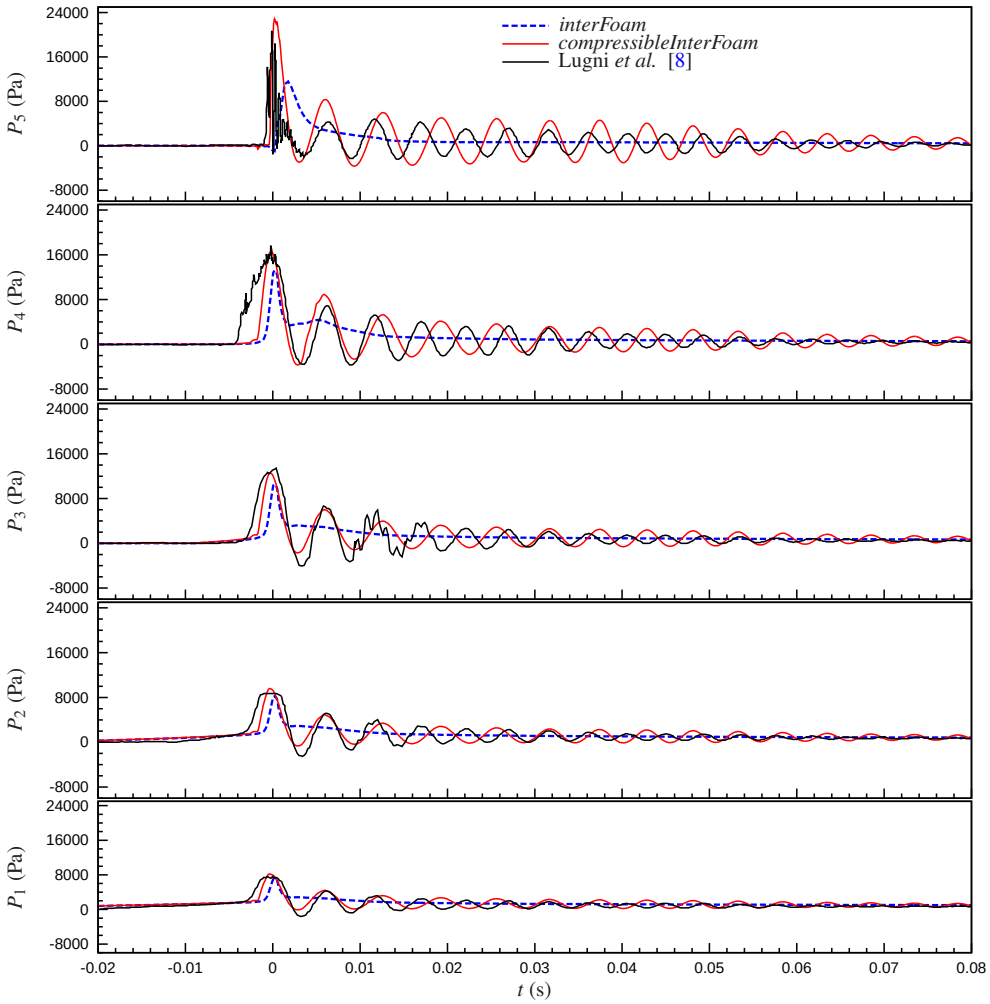

Figure 11: Pressure series at five different positions at the vertical wall of the tank. The black lines are experimental measurements of Lugni et al. [8]. The red lines are the present numerical results.

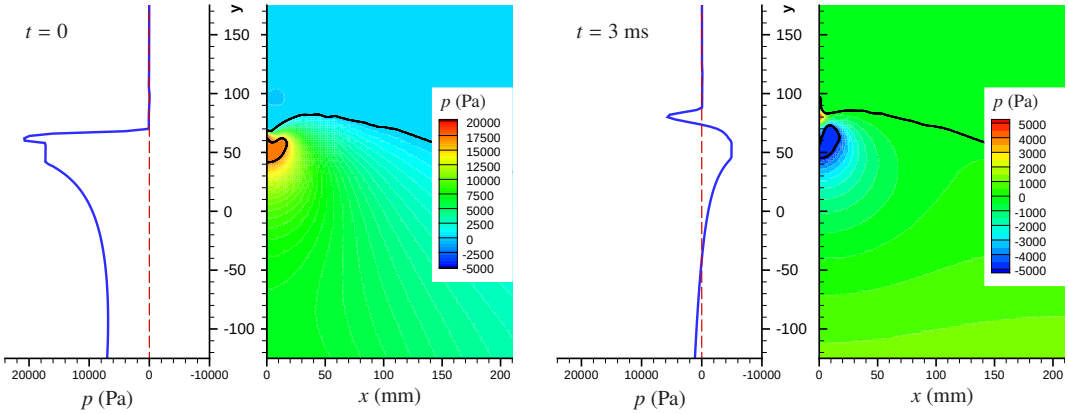

(a) First pressure peak

(b) First pressure trough

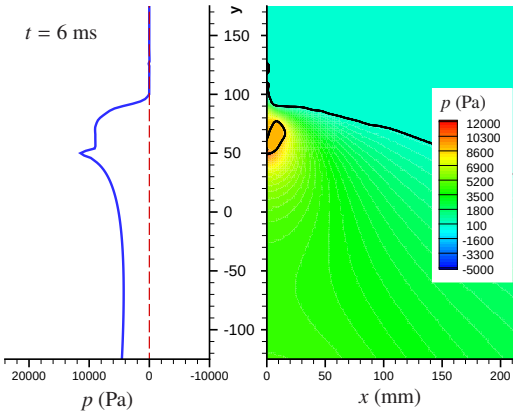

(c) Second pressure peak

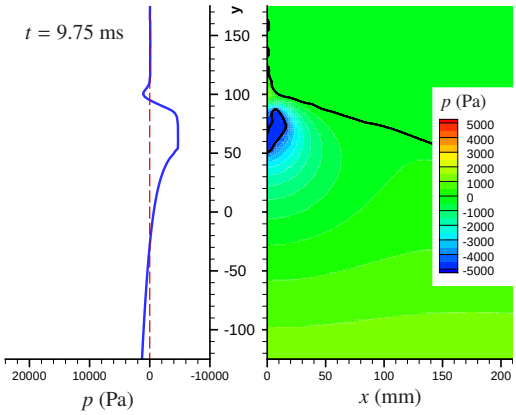

(d) Second pressure trough

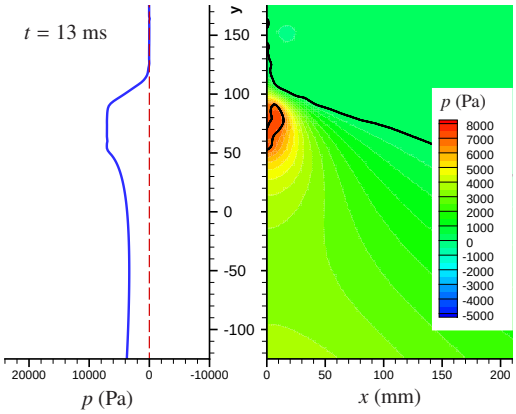

(e) Third pressure peak

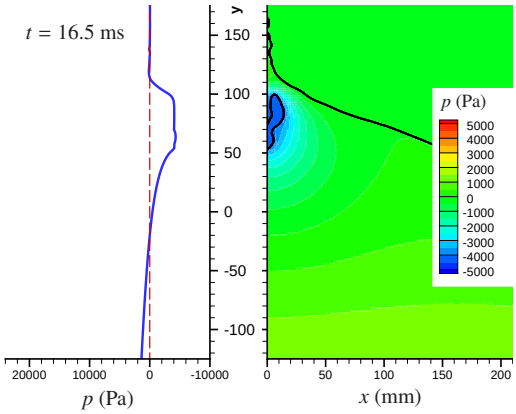

(f) Third pressure trough

Figure 12: Snapshots of the pressure field in the sloshing tank. At every time frame, the left part is the filled contours of gauge pressure (units in Pa) and the right part is its distribution along the vertical wall (units in mm). T_0 stands for the moment of the first pressure peak. Please note the different ranges of pressure in each filled contour graph.

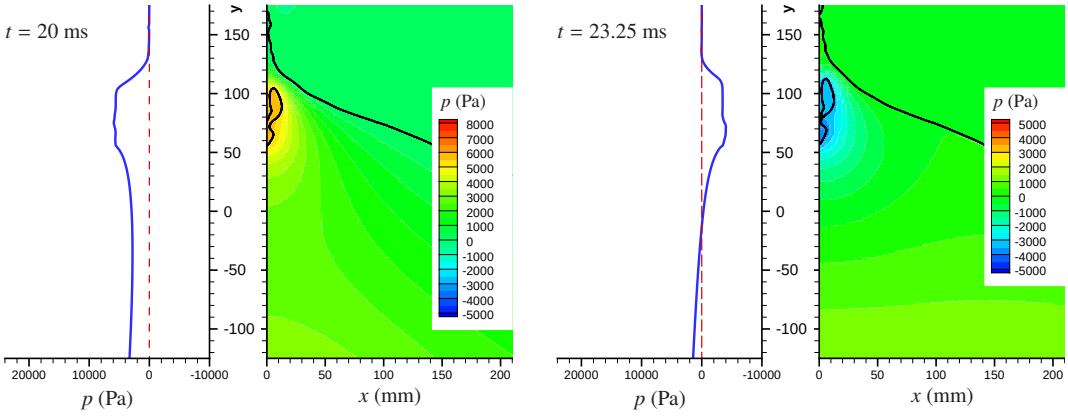

(g) Fourth pressure peak (h) Fourth pressure trough

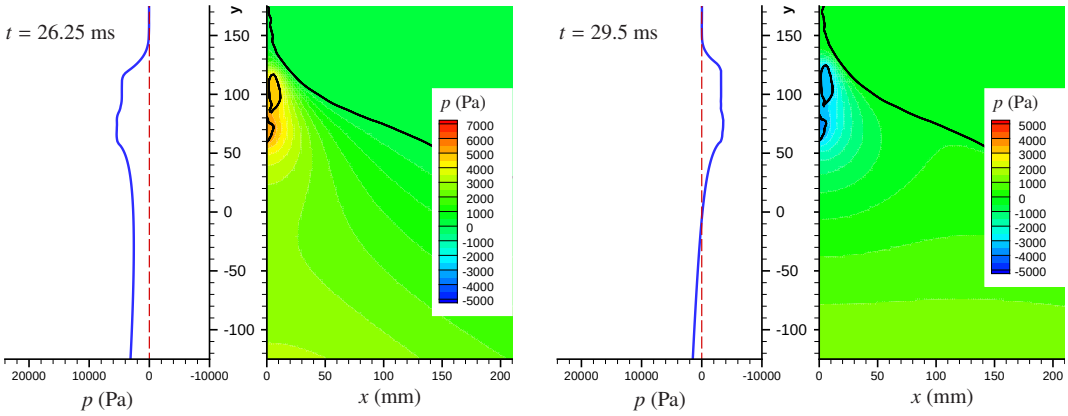

(i) Fifth pressure peak (j) Fifth pressure trough

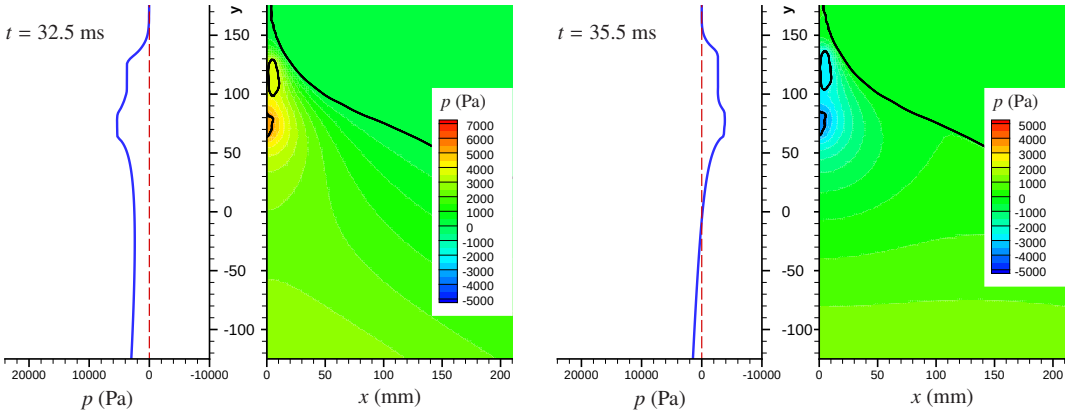

(k) Sixth pressure peak (l) Sixth pressure trough

Figure 12: Snapshots of the pressure field in the sloshing tank (cont.). At every time frame, the left part is the distribution of the gauge pressure (units in Pa) along the vertical wall (units in mm) and the right part is the filled contours of gauge pressure in the tank near the impact wall. The time $t = 0$ stands for the occurrence of the first pressure peak. Please note the different ranges of pressure in each filled contour graph.

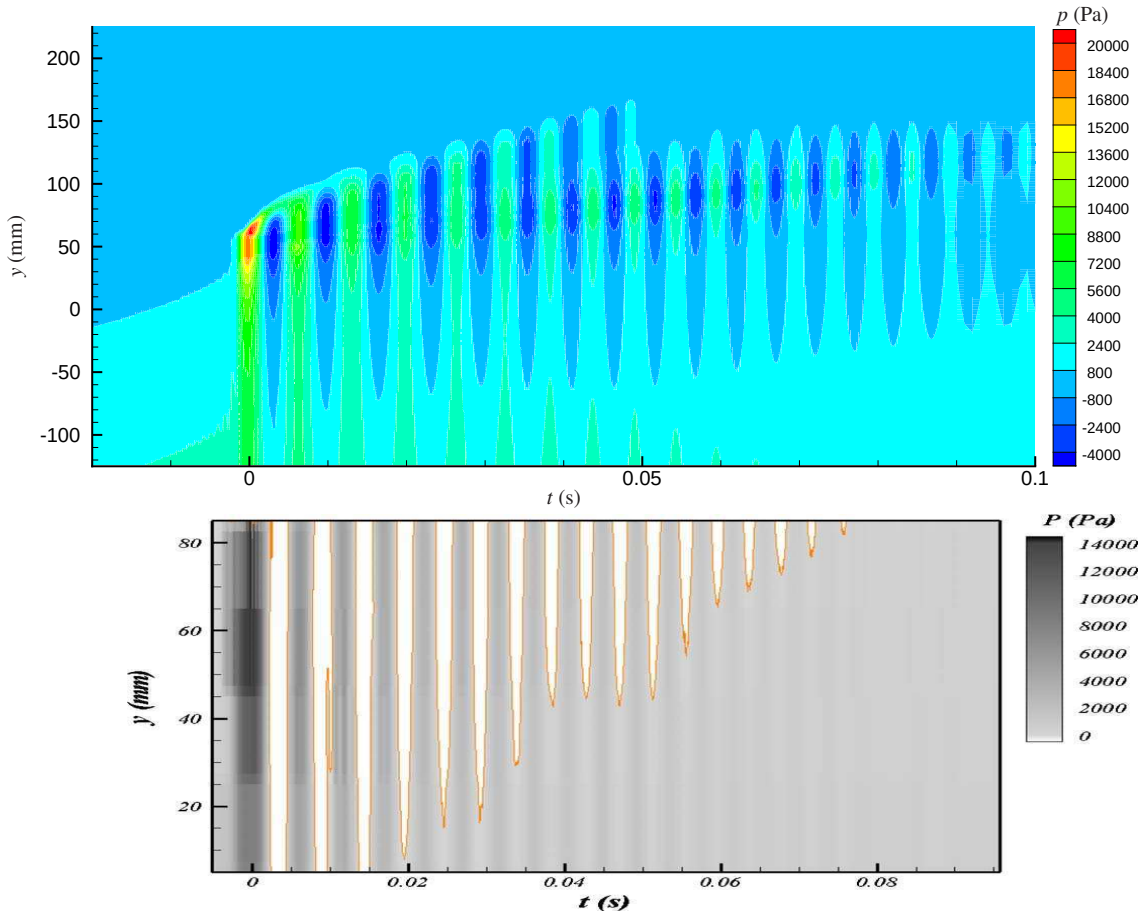

Figure 13: History of the gauge pressure on the vertical wall (Upper: numerical results computed by *compressibleInterFoam*; Lower: experimental results of Lugni *et al.* [8]). In the upper graph, the dark blue areas represent computed negative pressure loadings in coincidence with the expansion of the trapped air pocket. In the lower graph, the (dark) grey areas represent measured positive pressures; the white parts indicate negative pressures.

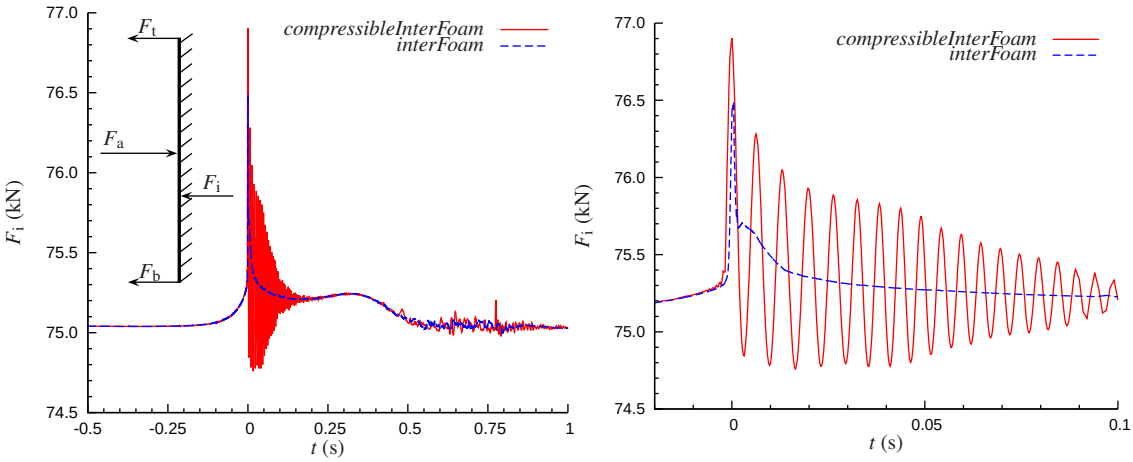

Figure 14: Wave induced horizontal impact force on the wall for time near the occurrence of plunging wave. The impact force is calculated by $F_{\mathrm{i}} = (\int_0^1 p_{\mathrm{impact}} \mathrm{d}y) L_z$, $L_z = 1$ m. F_{a} is the external atmospheric force on the wall. F_{t} and F_{b} are the friction provided by the ceiling and floor of the tank. Left: $t = -0.5 \sim 1$s; right: $t = -0.02 \sim 0.1$s.

thermodynamic behaviour of air enclosed wave impact problems other innovative ways are required accurately to measure the temperature with a high sample rate of no less than 2 kHz if ten sampling points are requested within just 5 ms. Though this goal is beyond the scope of the current study, our efforts through the present numerical modelling provides a view of the problem and a judgement of the necessary sample rate.

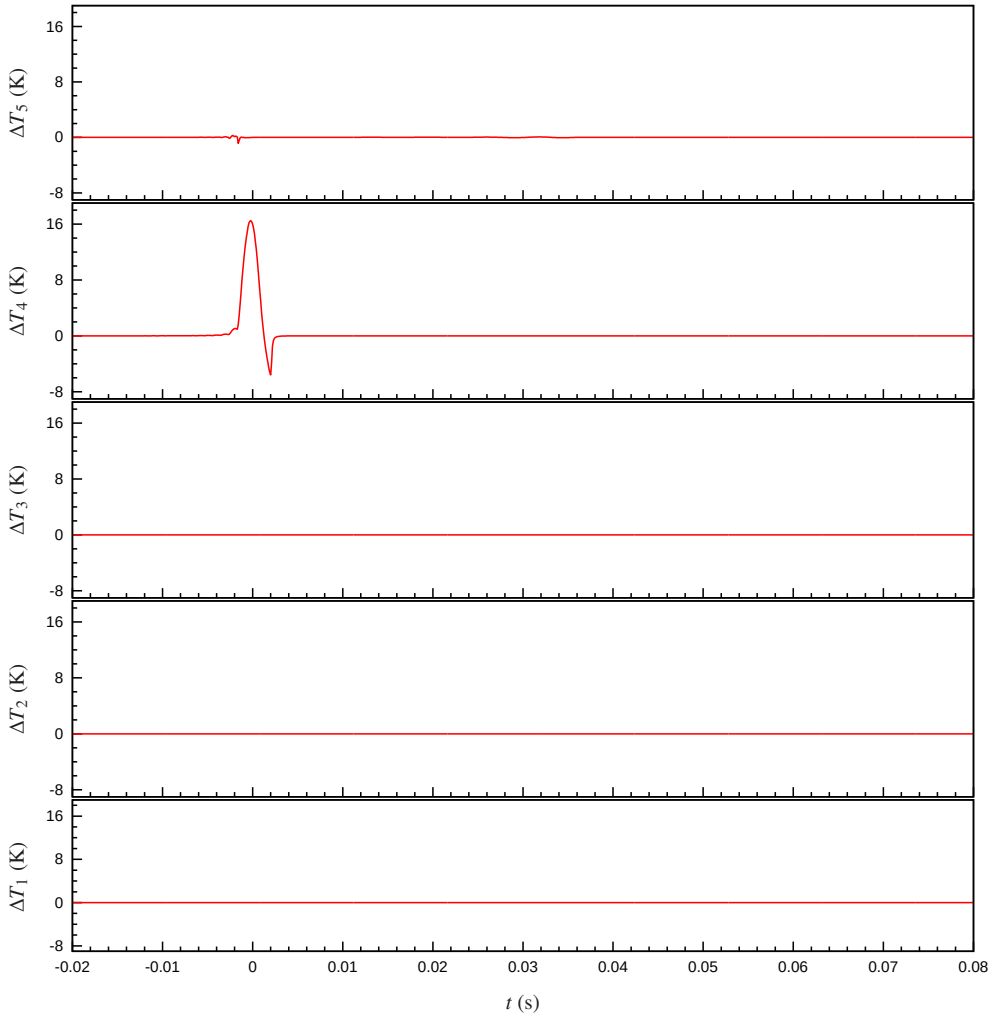

Figure 15: Time series of temperature variation at five different positions $P_1 \sim P_5$ (from bottom to top) on the vertical wall of the tank (computed by *compressibleInterFoam*). The initial temperature is set as $T = 15°C$ in the tank.

5. Conclusions

A numerical study has been carried out to investigate a plunging wave impact event in a low-filling depressurised sloshing tank using an open-source compressible two-phase flow code. The compressible code is firstly validated against experiments and other independent numerical methods with a benchmark test of a half-filling smooth sloshing

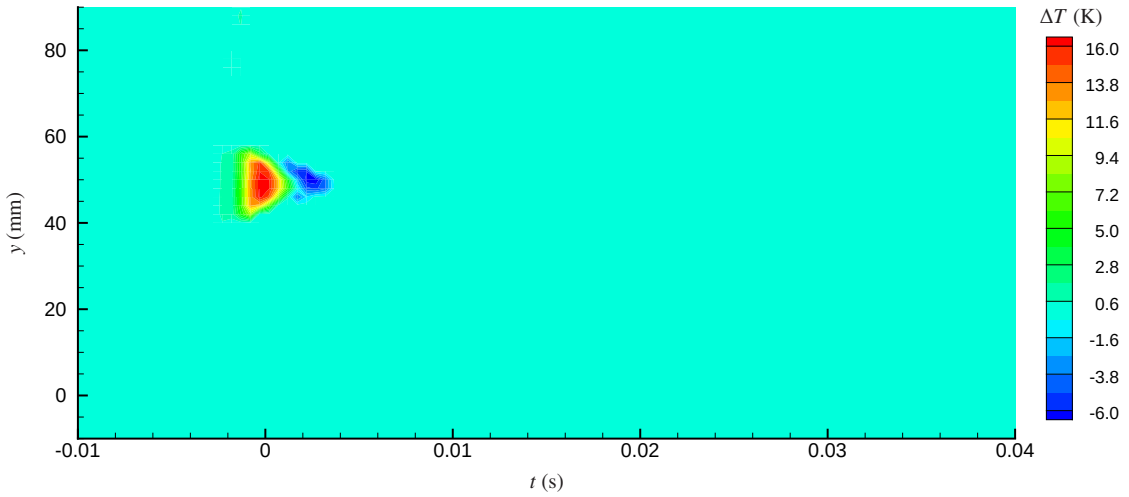

Figure 16: Temperature variations on the vertical wall (computed by *compressibleInterFoam*). The initial temperature is set as $T = 15°C$ in the tank.

tank. The converged pressures and free surface displacements calculated by the compressible code agree well with experimental and other numerical reference results. A careful inspection of numerical error reveals that the compressible code satisfies the mass conservation law quite well throughout the computations.

The compressible flow solver is then extended to calculate a violent sloshing wave in a low-filling tank. A detailed assessment of conservation error is carried out and the results show the good mass conservation property of the code. The computed free surface is similar to the experimental results. The complex phenomenon of an air pocket trapped in the body of a wave is successfully reproduced by the numerical model. The predicted pressures agree well with the experimental results regarding the amplitude and phase. The crucial pulsation of the pressure loadings in synchronisation with the contraction and expansion of the trapped air pocket is well handled by the compressible multiphase code, while an incompressible two-phase code failed substantially to resolve this complex physical phenomenon. This reveals that fluid compressibility is an extremely important factor for air-enclosed plunging wave impact problems, and it must be included and carefully handled by numerical models in order to reproduce the physical phenomena appropriately. Under this crucial compressiblity effect the fluid flow experiences both contraction and expansion which could lead to positive and negative gauge pressures alternately. In contrast to the infeasibility of using a load cell to measure the total fluid impact force on a vertical sloshing tank wall, the numerical model shows its advantage here to be able to obtain this important information in a relatively simple manner. The wave impact force integrated from the pressures also shows a strong pulsation in coincidence with the expansion and contraction of the trapped air pocket.

Exploratory investigation of the associated thermodynamics shows that the temperature remains almost constant in most areas in the tank. An exception is found in a rather confined area – the trapped air pocket, in which the temper-

ature has only one pulsation lasting for only about 5 ms. In order to disclose the real thermodynamic behaviour in an air enclosed plunging wave impact problem innovative techniques are needed to effectively measure the temperature accurately with a high frequency e.g. no less than 2 kHz if ten sampling points are demanded for the short thermal pulsation.

The current work focuses on the calculation of the main features of the air-enclosed plunging wave impacts. In future, attention will be paid to the local features e.g. break up of the water spray from the crest and free surface instabilities generated by the escaping air flow during the pocket enclosure which are greatly influenced by the viscosity and surface tension of the fluid. This will inevitably demand that an extremely fine mesh be used in order to capture the local features with satisfactory resolution.

Acknowledgements

The authors gratefully acknowledge financial support from the Engineering and Physical Sciences Research Council (EPSRC), U.K. under grant nos. EP/J010197/1, EP/J012793/1, EP/K037889/1 and EP/N008839/1. The authors are also very grateful to the anonymous reviewers for critiquing our work and providing constructive advice to improve the paper.

References

[1] W. Bai, X. Liu, C. Koh, Numerical study of violent lng sloshing induced by realistic ship motions using level set method, Ocean Eng. 97 (2015) 100–113. doi:10.1016/j.oceaneng.2015.01.010.

[2] G.-d. Xu, W.-y. Duan, Review of prediction techniques on hydrodynamic impact of ships, J. Mar. Sci. Appl. 8 (3) (2009) 204–210. doi:10.1007/s11804-009-8039-7.

[3] Y.-M. Scolan, M. Karimi, F. Dias, J.-M. Ghidaglia, J. Costes, Highly nonlinear wave in tank with small density ratio, in: 29th International Workshop on Water Waves and FloatingBodies, 2014.

[4] P. Lubin, S. Vincent, S. Abadie, J. Caltagirone, Three-dimensional large eddy simulation of air entrainment under plunging breaking waves, Coastal Eng. 53 (8) (2006) 631–655. doi:10.1016/j.coastaleng.2006.01.001.

[5] L. Qian, D. M. Causon, C. G. Mingham, D. M. Ingram, A free-surface capturing method for two fluid flows with moving bodies, Proc. R. Soc. A 462 (2006) 21–42. doi:10.1098/rspa.2005.1528.

[6] G. Bullock, C. Obhrai, D. Peregrine, H. Bredmose, Violent breaking wave impacts. part 1: Results from large-scale regular wave tests on vertical and sloping walls, Coastal Eng. 54 (8) (2007) 602–617. doi:10.1016/j.coastaleng.2006.12.002.

[7] E. Chan, W. Melville, E. Chan, W. Melville, Deep-water plunging wave pressures on a vertical plane wall, Proc. R. Soc. Lond. A 417 (1852) (1988) 95–131. doi:10.1098/rspa.1988.0053.

[8] C. Lugni, M. Brocchini, O. M. Faltinsen, Evolution of the air cavity during a depressurized wave impact. II. The dynamic field, Phys. Fluids 22 (5) (2010) 056102. doi:10.1063/1.3409491.

[9] C. Lugni, M. Miozzi, M. Brocchini, O. Faltinsen, Evolution of the air cavity during a depressurized wave impact. I. The kinematic flow field, Phys. Fluids 22 (2010) 056101. doi:10.1063/1.3407664.

[10] D. Peregrine, Water-wave impact on walls, Annu. Rev. Fluid Mech. 35 (1) (2003) 23–43. doi:10.1146/annurev.fluid.35.101101.161153.

[11] G. K. Kapsenberg, Slamming of ships: where are we now?, Phil. Trans. R. Soc. A 369 (1947) (2011) 2892–2919. doi:10.1098/rsta.2011.0118.

[12] H. Bredmose, D. Peregrine, G. Bullock, Violent breaking wave impacts. part 2: modelling the effect of air, J. Fluid Mech. 641 (1) (2009) 389–430. doi:10.1017/S0022112009991571.

[13] H. Bredmose, G. N. Bullock, A. J. Hogg, Violent breaking wave impacts. part 3. effects of scale and aeration, J. Fluid Mech. 765 (2015) 82–113. doi:10.1017/jfm.2014.692.

[14] L.-R. Plumerault, D. Astruc, P. Villedieu, P. Maron, A numerical model for aerated-water wave breaking, Int. J. Numer. Methods Fluids 69 (12) (2012) 1851–1871. doi:10.1002/fld.2667.

[15] L.-R. Plumerault, D. Astruc, P. Maron, The influence of air on the impact of a plunging breaking wave on a vertical wall using a multifluid model, Coastal Eng. 62 (2012) 62–74. doi:10.1016/j.coastaleng.2011.12.002.

[16] Z. H. Ma, D. M. Causon, L. Qian, C. G. Mingham, H. B. Gu, P. M. Ferrer, A compressible multiphase flow model for violent aerated wave impact problems, Proc. R. Soc. A 470 (2172) (2014) 20140542. doi:10.1098/rspa.2014.0542.

[17] Z. H. Ma, D. M. Causon, L. Qian, H. Gu, C. G. Mingham, P. M. Ferrer, A GPU based compressible multiphase hydrocode for modelling violent hydrodynamic impact problems, Computers and Fluids 120 (2015) 1–23. doi:10.1016/j.compfluid.2015.07.010.

[18] Z. H. Ma, D. M. Causon, L. Qian, C. G. Mingham, T. Mai, D. Greaves, A. Raby, Pure and aerated water entry of a flat plate, Physics of Fluids 28 (2016) 016104. doi:10.1063/1.4940043.

[19] S. Y. Kadioglu, M. Sussman, S. Osher, J. P. Wright, M. Kang, A second order primitive preconditioner for solving all speed multi-phase flows, J. Comput. Phys. 209 (2) (2005) 477–503. doi:10.1016/j.jcp.2005.03.020.

[20] S. LeMartelot, B. Nkonga, R. Saurel, Liquid and liquid–gas flows at all speeds, J. Comput. Phys. 255 (2013) 53–82. doi:10.1016/j.jcp.2013.08.001.

[21] D. van der Heul, C. Vuik, P. Wesseling, A conservative pressure-correction method for flow at all speeds, Computers & Fluids 32 (8) (2003) 1113–1132. doi:10.1016/s0045-7930(02)00086-5.

[22] K. S. Shterev, S. K. Stefanov, Pressure based finite volume method for calculation of compressible viscous gas flows, J. Comput. Phys. 229 (2) (2010) 461–480. doi:10.1016/j.jcp.2009.09.042.

[23] Z. Chen, A. Przekwas, A coupled pressure-based computational method for incompressible/compressible flows, J. Comput. Phys. 229 (24) (2010) 9150–9165. doi:10.1016/j.jcp.2010.08.029.

[24] I. Senocak, W. Shyy, A pressure-based method for turbulent cavitating flow computations, J. Comput. Phys. 176 (2) (2002) 363–383. doi:10.1006/jcph.2002.6992.

[25] A. Colagrossi, M. Landrini, Numerical simulation of interfacial flows by smoothed particle hydrodynamics, Journal of Computational Physics 191 (2) (2003) 448–475. doi:10.1016/s0021-9991(03)00324-3.

[26] A. Colagrossi, C. Lugni, M. Brocchini, A study of violent sloshing wave impacts using an improved SPH method, Journal of Hydraulic Research 48 (sup1) (2010) 94–104. doi:10.1080/00221686.2010.9641250.

[27] P. Guilcher, Y. Jus, N. Couty, L. Brosset, Y.-M. Scolan, D. Le Touzé, et al., 2D simulations of breaking wave impacts on a flat rigid wall–part 1: Influence of the wave shape, in: The Twenty-fourth International Ocean and Polar Engineering Conference, International Society of Offshore and Polar Engineers, 2014, pp. 232–245.

[28] P.-M. Guilcher, N. Couty, L. Brosset, D. Le Touzé, et al., Simulations of breaking wave impacts on a rigid wall at two different scales with a two-phase fluid compressible SPH model, International Journal of Offshore and Polar Engineering 23 (04) (2013) 241–253.

[29] A. Rafiee, D. Dutykh, F. Dias, Numerical simulation of wave impact on a rigid wall using a twophase compressible SPH method, Procedia IUTAM 18 (2015) 123–137. doi:10.1016/j.piutam.2015.11.013.

[30] R. Issa, Solution of the implicitly discretised fluid flow equations by operator-splitting, J. Comput. Phys. 62 (1) (1986) 4065. doi:10.1016/0021-9991(86)90099-9.
URL http://dx.doi.org/10.1016/0021-9991(86)90099-9

[31] C. G. Koh, M. Gao, C. Luo, A new particle method for simulation of incompressible free surface flow problems, Int. J. Numer. Meth. Engng 89 (12) (2011) 1582–1604. doi:10.1002/nme.3303.

[32] B. C. Abrahamsen, O. M. Faltinsen, The effect of air leakage and heat exchange on the decay of entrapped air pocket slamming oscillations, Phys. Fluids 23 (10) (2011) 102107. doi:10.1063/1.3638612.